Active Disturbance Rejection Formation Control for Multiagent Systems with Input Constraints

Caoyuan Gu, Xiang Wu, Wen-An Zhang, *Member, IEEE*, Hongjie Ni, and Steven X. Ding

***Abstract*—This paper deals with formation control of multiagent systems (MASs) subject to disturbances and input constraints, and an active disturbance rejection formation control (ADRFC) approach based on distributed observation is proposed. Firstly, the states and disturbances of tracking error systems are estimated by a distributed intermediate estimator (DIE). Secondly, an improved distributed model predictive control (IDMPC) is proposed to achieve formation control of MASs under disturbances and input constraints. Then, the robust ADRFC method is designed by combining the DIE and IDMPC, and the stability of the whole system is analyzed. Finally, experiments are conducted on a MAS consisting of four mobile robots to illustrate the effectiveness and superiority of the proposed method.**

***Index Terms*—Multiagent systems, disturbance rejection, intermediate estimator, model predictive control, formation control**

I. Introduction

In recent years, multiagent systems (MASs) [1], [2] have received more and more attention due to their wide applications in the fields of intelligent detection [3], logistics and transportation [4], disaster relief [5] and other areas. Then, as one of the main applications of MASs, formation control tasks [6] become a major research hotspot, and a variety of formation control methods have been designed, such as leader-follower-based [7], virtual structure-based [8], and behavior-based methods [9]. On the other hand, disturbances caused by modeling uncertainties, aging and wear of components, environmental noise, and many other factors are another troublesome issue in the formation control task of MASs. Furthermore, disturbances in any agent can spread to the whole system through the communication topology, which may seriously deteriorate the system performance or even destabilize the MAS.

To solve the disturbance problem, active disturbance rejection techniques based on disturbance observer or estimator become capable ways, because they have two degrees of freedom without sacrificing the control performance of the nominal system [10]. Then, disturbance observer (DOB) [11]–[13], extended state observer (ESO) [14]–[17], equivalent input observer (EID) [18], [19], intermediate estimator (IE) [20] and many other disturbance observer-based techniques have been widely studied and applied. Notably, compared to the common existing observers, intermediate estimator do not need to satisfy the observer matching condition. Moreover, the intermediate estimator can directly quantify the convergence speed by adjusting the observer parameter. In fact, the speed and accuracy of fault estimation can be improved by directly tuning the parameter [20]. Thereby, it has been widely used in MASs and obtained excellent performance [21], [22].

In the formation control task of MASs, distributed model predictive control (DMPC) is a highly effective approach [23]–[25]. By introducing a cost function and solving a series of distributed optimization problems, the optimal control law for each agent can be obtained. Furthermore, considering the disturbances rejection issue of formation control for MASs, disturbance estimation information is added to the control law of DMPC to achieve robust control performance [26], [27]. However, to the best of our knowledge, there are usually control input constraints in practical MAS considering the performance and security of hardware devices, which leads to the fact that some of the above methods cannot be applied in practical devices. Meanwhile, the stability of these methods proves to be simpler and does not analyze the terminal constraint set and terminal penalty matrix of DMPC in detail. In addition, the formation control and the disturbance rejection of existing methods are essentially two separate parts [27]–[29], which reduces the control performance of the system. As mentioned above, there is still no effective method that can organically combine formation control and disturbance rejection technique to address the formation control task of MASs with input constraints and disturbances.

Motivated by the above discussion, this paper reconstructs the distributed intermediate estimator (DIE) and proposes an improved distributed model predictive control (IDMPC). Furthermore, an active disturbance rejection formation control (ADRFC) method is proposed for MAS by integrating DIE and IDMPC. The contributions of this paper are threefold:

1) Compared with the nominal DIE in [21], an observer gain minimization strategy is designed under the premise of guaranteeing the DIE estimation performance. The phenomenon of controller oscillation due to too large observer gain after adding a correction term to the IDMPC prediction equation is avoided.
2) An IDMPC strategy is proposed to handle the input constraints issue of the actual actuator of MASs. By maximizing the terminal constraint set and minimizing the terminal penalty matrix, a suitable controller can be obtained to efficiently perform path tracking and formation synchronization tasks.
3) Integrated formation controller is designed by incorporating DIE and IDMPC. A rigorous stability analysis of the proposed ADRFC approach is given. The controller is able to automatically trade-off between formation con-

C. Gu, X. Wu, W.-A. Zhang and H. Ni are all with the Automatic Department, Zhejiang University of Technology, Hangzhou, 310023, China. (Corresponding author: Wen-An Zhang, e-mail: wazhang@zjut.edu.cn;)

S. X. Ding is with the Institute for Automatic Control and Complex Systems (AKS), University of Duisburg-Essen, 47057 Duisburg, Germany.

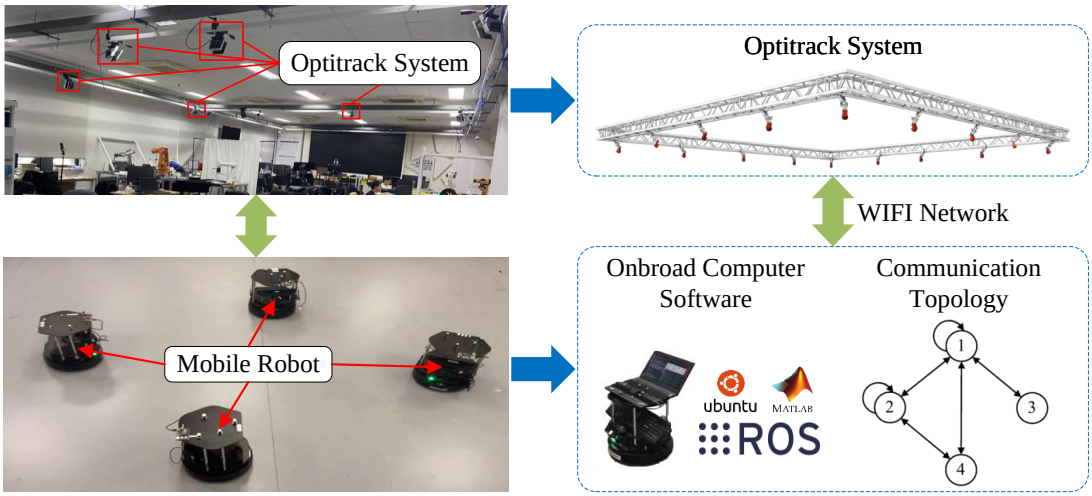

Fig. 1. MAS experimental platform and communication topology

trol and disturbance rejection and improves the transient performance of the system. In addition, experiments are conducted with four mobile robots to verify the effectiveness and superiority of ADRFC.

II. MAS and Problem Formulation

In this paper, a typical MAS experimental platform consisting of four TurtleBot-2 mobile robots is constructed, as shown in Fig. 1. This mobile robot has a two-wheel differential layout, and its maximum linear and angular velocities are 0.7 m/s and 3.14 rad/s, respectively. In addition, the robot is positioned by a set of wraparound digital camera OV7620, which is a 1/3-inch CMOS image sensor with an image resolution of 320*240 at 300 dots per inch. Therefore, the smallest displacement that can be recognized by this camera is 2.54cm/300=0.0085cm. The sampling period is set to $T_s = 0.05s$. The communication topology associated with the four mobile robots is undirected. The adjacency matrix is represented by $\mathcal{A} = \{a_{ij}\}$ with $a_{ii} = 0$. If agent i can receive information from agent j, $a_{ij} = 1$; otherwise, $a_{ij} = 0$. The involved pinning matrix is indicated as $G = \text{diag}\{g_i\} \in \mathbb{R}^{N\times N}$, where $g_i = 1$ if node i exchanges information with itself.

Considering that MAS forms a concentric circle formation around an object, which is a typical formation task such as in [30] and [31]. Then, Fig. 2 displays the desired circle formation based on the virtual structure approach, where VMR denotes the virtual mobile robot and MR denotes the mobile robot. Define $\mathbf{V}_i = (x_{vi}, y_{vi}, \theta_{vi})$ be the position (x_{vi}, y_{vi}) and directional angle θ_{vi} of VMR. Similarly, for MR i, denote $\mathbf{A}_i = (x_{ai}, y_{ai}, \theta_{ai})$, where (x_{ai}, y_{ai}) is position and θ_{ai} is the direction angle. The MRs need to track the reference trajectory Γ_i generated by the VMRs, $i = 1, \ldots, N$. As shown in Fig. 2, the four MRs need to form a formation of concentric circles with radius $2m$, and the ideal angle differences between two adjacent MRs are $\theta_{12}^r = \theta_{23}^r = \theta_{34}^r = \frac{\pi}{4}$. Then, the kinematic model of the VMR i and its corresponding MR can be obtained

$$\dot{\phi}_{vi} = \begin{bmatrix} \dot{x}_{vi} \\ \dot{y}_{vi} \\ \dot{\theta}_{vi} \end{bmatrix} = \begin{bmatrix} \cos\theta_{vi} & 0 \\ \sin\theta_{vi} & 0 \\ 0 & 1 \end{bmatrix} \begin{bmatrix} v_{vi} \\ \omega_{vi} \end{bmatrix}, \tag{1}$$

$$\dot{\phi}_{ai} = \begin{bmatrix} \dot{x}_{ai} \\ \dot{y}_{ai} \\ \dot{\theta}_{ai} \end{bmatrix} = \begin{bmatrix} \cos\theta_{ai} & 0 \\ \sin\theta_{ai} & 0 \\ 0 & 1 \end{bmatrix} \begin{bmatrix} v_{ai} \\ \omega_{ai} + f_{di} \end{bmatrix}, \tag{2}$$

where v_{vi} and ω_{vi} represent the linear and angular velocities of the VMR i, respectively. v_{ai} and ω_{ai} are the linear velocity and angular velocity of the MR i, respectively. The effects of modeling uncertainty, component aging and wear, and environmental noise on the system are considered as the total disturbance f_{di}. It is assumed that f_{di} belongs to the L_2 norm bounded function and its increment satisfies $\|\Delta f_{di}(k)\| \leq \theta_f$.

Remark 1: As can be seen from (2), the displacement of the robot in the X and Y directions is determined by the orientation angle θ_{ai} and the linear velocity v_{vi}, and if there is a linear velocity disturbance, the disturbance effect can be eliminated by adjusting the orientation angle of the robot. In contrast, the orientation angle of the robot is only determined by the angular velocity, and the disturbance occurring in the angular velocity cannot be compensated by the change in X and Y directions. Therefore, angular velocity disturbance has a more significant effect on the trajectory of the mobile robot compared to linear velocity disturbance, which is the reason why only angular velocity disturbance is considered in this paper.

Based on the framework of path coordinates, the tracking error state ϕ_{ei} between $\mathbf{V}_i$ and $\mathbf{A}_i$ in the global coordinate system can be converted to the local coordinate system

$$\phi_{ei} = \begin{bmatrix} x_{ei} \\ y_{ei} \\ \theta_{ei} \end{bmatrix} = \begin{bmatrix} \cos\theta_{ai} & \sin\theta_{ai} & 0 \\ -\sin\theta_{ai} & \cos\theta_{ai} & 0 \\ 0 & 0 & 1 \end{bmatrix} (\mathbf{V}_i - \mathbf{A}_i). \tag{3}$$

By taking the derivative of (3) and rearranging with kinematic model, one obtains

$$\begin{cases} \dot{x}_{ei} = \omega_{ai} y_{ei} - v_{ai} + v_{vi}\cos\theta_{ei}, \\ \dot{y}_{ei} = -\omega_{ai} x_{ei} + v_{vi}\sin\theta_{ei}, \\ \dot{\theta}_{ei} = \omega_{vi} - (\omega_{ai} + f_{di}). \end{cases} \tag{4}$$

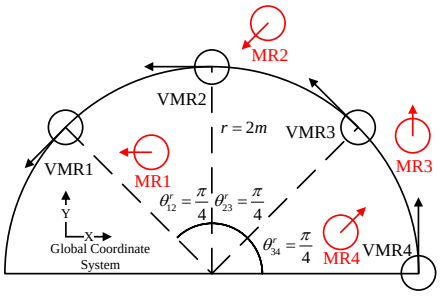

Fig. 2. Desired formation for MAS

By linearizing (4) around the equilibrium point [27], and discretize it according to the sampling period T_s. Define $u_{ei} = \left[\begin{array}{cc} v_{vi}\cos\theta_{ei} - v_{ai} & \omega_{vi} - \omega_{ai} \end{array} \right]^{\mathrm{T}}$, the dynamics of the tracking error system i in the local coordinate system can be obtained as

$$\begin{cases} \phi_{ei}(k+1) = A_e\phi_{ei}(k) + B_e u_{ei}(k) + B_f f_{di}(k), \\ y_{ei}(k) = C_e\phi_{ei}(k), \end{cases} \tag{5}$$

where $\phi_{ei}(k) \in \mathbb{R}^n$, $u_{ei}(k) \in \mathbb{R}^m$, $y_{ei}(k) \in \mathbb{R}^p$ and $f_{di}(k)$, represent the tracking error system state, the control input, the measurement output and the disturbance, respectively. The coefficient matrices are given as follows

$$A_e = \left[\begin{array}{ccc} 1 & T_s\omega_{vi} & 0 \\ -T_s\omega_{vi} & 1 & T_s v_{vi} \\ 0 & 0 & 1 \end{array} \right], B_e = \left[\begin{array}{cc} T_s & 0 \\ 0 & 0 \\ 0 & T_s \end{array} \right],$$

$$B_f = B_e H_1, H_1 = \left[\begin{array}{c} 0 \\ -1 \end{array} \right], C_e = \left[\begin{array}{ccc} 1 & 0 & 0 \\ 0 & 1 & 0 \\ 0 & 0 & 1 \end{array} \right].$$

Considering the formation control problem of MAS, the reference path Γ_i generated by the VMR is parameterized by the variable θ_{vi}. Then, the state of the parameterized path of MR i is given as $\Gamma_i(\theta_{vi}) = \left[\begin{array}{ccc} x_{vi}(\theta_{vi}) & y_{vi}(\theta_{vi}) & \theta_{vi} \end{array} \right]^{\mathrm{T}}$. According to (1), the path variable θ_{vi} can be expressed as

$$\theta_{vi}(k+1) = \theta_{vi}(k) + T_s\omega_{vi}(k). \tag{6}$$

It can be seen that if all path parameters θ_{vi} reach consensus, such as $\theta_{vi}(k) - \theta_{vj}(k) - \theta_{ij}^r = 0$, $i \neq j$, then the VMR will be at the desired position of the geometric structure. The MRs will be able to track the VMRs and form the desired formation. Thus, the formation control problem for the MAS in the presence of disturbances can be decomposed into the following two tasks.

1) **Path tracking task:** To ensure that each MR can converge to the corresponding VMR and move along the path of Γ_i in the presence of disturbance and input constraint. It is necessary to design a controller for each MR such that the following condition holds

$$\lim_{k\to\infty} \|\phi_{ei}(k)\| = 0. \tag{7}$$

2) **Formation synchronization task:** To ensure that all MR path parameters $\theta_{ai}(k), i = 1, ..., N$ are synchronized in the presence of disturbance and input constraint to maintain the desired formation. It is necessary to design a controller for each MR to achieve the following objective, i.e.,

$$\lim_{k\to\infty} \left\|\theta_{ai}(k) - \theta_{aj}(k) - \theta_{ij}^r\right\| = 0. \tag{8}$$

To summarize, the main objective of this paper is to design an ADRFC method for MASs with disturbances and input constraints. Thus, it is ensured that each MR and its corresponding path are synchronized, and a desired formation is achieved.

III. Design of ADRFC for MAS

In this section, an ADRFC approach is designed by incorporating DIE and IDMPC. Then, the design of the DIE and IDMPC are given in Section III.A and III.B, respectively. Subsequently, the integrated formation controller (Section III.C) and the stability analysis (Section III.D) are presented.

A. DIE for Disturbance Estimation

In order to estimate the states and disturbances of the system, a set of DIEs are constructed, the structural assumptions of the DIE are given in [21]. The following intermediate variable is defined as

$$\delta_i(k) = f_{di}(k) - \varpi B_f^T \phi_{ei}(k), \tag{9}$$

where ϖ is an adjustable parameter. Then, for the i-th MR, the DIE is presented as

$$\begin{cases} \hat{\phi}_{ei}(k+1) = A_e\hat{\phi}_{ei}(k) + B_e u_{ei}(k) + B_f\hat{f}_{di}(k) \\ \qquad\qquad +HY_{ei}(k), \\ \hat{\delta}_i(k+1) = \hat{f}_{di}(k) - \varpi B_f^T A_e\hat{\phi}_{ei}(k) \\ \qquad\qquad -\varpi B_f^T B_e u_e(k) - \varpi B_f^T B_f\hat{f}_{di}(k), \\ \hat{f}_{di}(k) = \hat{\delta}_i(k) + \varpi B_f^T\hat{\phi}_{ei}(k), \\ \hat{y}_{ei}(k) = C_e\hat{\phi}_{ei}(k), \end{cases} \tag{10}$$

where $Y_{ei}(k) = (\sum_{j\in N} a_{ij}(y_{ei}(k) - y_{ej}(k)) + g_i y_{ei}(k) - \sum_{j\in N} a_{ij}(\hat{y}_{ei}(k) - \hat{y}_{ej}(k)) - g_i\hat{y}_{ei}(k))$. H is the observer gain to be solved. $\hat{\phi}_{ei}(k)$, $\hat{\delta}_i(k)$, $\hat{f}_{di}(k)$ and $\hat{y}_{ei}(k)$ are the estimates of $\phi_{ei}(k)$, $\delta_i(k)$, $f_{di}(k)$ and $y_{ei}(k)$, respectively.

Define the estimation errors $e_{\phi i}(k) = \phi_{ei}(k) - \hat{\phi}_{ei}(k)$ and $e_{\delta i}(k) = \delta_i(k) - \hat{\delta}_i(k)$, $A_1 = \left(A_e + \varpi B_f B_f^T\right)$, $A_2 = \varpi B_f^T\left(I - A_e - \varpi B_f B_f^T\right)$, $A_3 = \left(I - \varpi B_f^T B_f\right)$, the overall estimation error system can be expressed as

$$\begin{aligned} e_\phi(k+1) =& (I_N \otimes A_1) e_\phi(k) - (M \otimes HC) e_\phi(k) \\ &+ (I_N \otimes B_f) e_\delta(k), \end{aligned} \tag{11}$$

$$\begin{aligned} e_\delta(k+1) =& (I_N \otimes A_2) e_\phi(k) + (I_N \otimes A_3) e_\delta(k) \\ &+ (I_N \otimes I)\Delta f_d(k), \end{aligned} \tag{12}$$

where $\otimes$ denotes Kronecker product, $M = L + G$, L is the Laplacian matrix, $e_\phi(k) = \left[e_{\phi_1}^T(k), \ldots, e_{\phi_N}^T(k)\right]^T$, $e_\delta(k)$ and $\Delta f_d(k)$ are similar to $e_\phi(k)$. The DIE utilizes the output difference $HY_{ei}(k)$ between the controlled object and the observation system to correct the estimated value, and the convergence of the state observation error (11) and the intermediate variable observation error (12) can be ensured by the proper configuration of the gain matrix H. Subsequently, the stability of the overall estimation error system and the observer gain can be obtained from the following theorem [21].

***Theorem** 1:* The states of the overall estimation error system (11)-(12) are uniformly ultimately bounded if there exist scalars $\varpi > 0$, matrices $P_1 > 0$, $P_2 > 0$ and $W > 0$, such that the following optimization problem is solvable

$$\begin{aligned} \min \quad & -\log\left(\det P_1\right) \\ s.t. \quad & \begin{bmatrix} \Theta_{11}^i & \Theta_{12}^i & \Theta_{13}^i & \Theta_{14}^i & 0 \\ * & \Theta_{22}^i & 0 & 0 & \Theta_{25}^i \\ * & * & \Theta_{33}^i & 0 & 0 \\ * & * & * & -\varepsilon I & 0 \\ * & * & * & * & -\varepsilon I \end{bmatrix} < 0 \end{aligned} \tag{13}$$

where $i = 1, 2, ..., N$, λ_i is the eigenvalue of M, the symbol $*$ within a matrix represents the symmetric entry. $\Theta_{11}^i = A_2^T P_2 A_2 - P_1$, $\Theta_{12}^i = A_1^T P_1 B_f - \lambda_i C^T W^T B_f + A_2^T P_2 A_3$, $\Theta_{13}^i = A_1^T P_1 - \lambda_i C^T W^T$, $\Theta_{14}^i = A_2^T P_2$, $\Theta_{22}^i = B_f^T P_1 B_f + A_3^T P_2 A_3 - P_2$, $\Theta_{25}^i = A_3^T P_2$, $\Theta_{33}^i = -P_1$. Then, the gain of the DIE is given by $H = P_1^{-1} W$.

***Proof*:** Please See the Appendix.A.

***Remark** 2:* In [21], H is a feasible solution for the stability linear matrix inequality. Due to the use of state feedback, the magnitude of H is not directly related to the performance of the control law. In this paper, the control law obtained from the IDMPC solution is used and the error correction term $HY_{ei}(k)$ is added to the prediction equation. Therefore, it is necessary to limit the magnitude of H to prevent system oscillations. Here, $-\log\left(\det P_1\right)$ is selected as the optimization objective.

B. IDMPC with Input Constraint

In the existing DMPC-based results [32], [33], the terminal constraint set and the terminal penalty matrix are obtained directly from a Lyapunov equation, which cannot handle the impact of the input constraints on the system well. Therefore, an IDMPC is designed to ensure that each MR can perform path tracking and formation synchronization tasks. The local cost function of the i-th MR is as follows

$$\begin{aligned} J_i(k) = \sum_{l=0}^{P-1} \Bigg(& \left\| \hat{\phi}_{ei}(k+l\,|k) \right\|_Q^2 + \left\| u_{ei}(k+l\,|k) \right\|_R^2 \\ & + \Big(\sum_{j \in N} a_{ij} H_2 \left(\hat{\phi}_{ej}(k+l\,|k) - \hat{\phi}_{ei}(k+l\,|k) \right) \\ & - g_i H_2 \hat{\phi}_{ei}(k+l\,|k) \Big)^2 \Bigg) + \left\| \hat{\phi}_{ei}(k+P\,|k) \right\|_{P_4}^2, \end{aligned} \tag{14}$$

where $H_2 = \begin{bmatrix} 0 & 0 & 1 \end{bmatrix}^{\mathrm{T}}$, P is the prediction horizon, $\hat{\phi}_{ei}(k+l\,|k)$ and $u_{ei}(k+l\,|k)$ represent the prediction value of the $\hat{\phi}_{ei}(k\,|k)$ and $u_{ei}(k\,|k)$ at time k, respectively. Q and R are both real, symmetric positive definite weight matrices trading-off control cost for better system performance. P_4 is a terminal penalty matrix.

***Remark** 3:* As shown in Eq. (14), the cost function proposed in this paper can be divided into four components. The first two components, $\left\| \hat{\phi}_{ei} \right\|_Q^2$ and $\left\| u_{ei} \right\|_R^2$ represent the costs associated with the system state and control inputs respectively, which ensure that each MR converges to its corresponding VMR. $\big(\sum_{j \in N} a_{ij} H_2 \left(\hat{\phi}_{ej} - \hat{\phi}_{ei} \right) - g_i H_2 \hat{\phi}_{ei} \big)^2$ denotes the cost of the directional angle between MRs for the formation synchronization task. Moreover, $\left\| \hat{\phi}_{ei} \right\|_{P_4}^2$ is the terminal penalty that guarantees the system trajectory converges to the terminal constraint set.

***Remark** 4:* Note that g_i = 1 denotes the interaction of own information, and this symbol appears mainly in two places: 1) The $g_i(y_{ei}(k) - \hat{y}_{ei}(k))$ in the DIE design process (10). Its main function is to ensure the convergence of the output error and output error estimation of the MR itself. 2) The $g_i H_2 \hat{\phi}_{ei}(k+l\,|k)$ in the IDMPC cost function (14), whose main function is to ensure the convergence of the tracking error of the MR itself. The g_i in the DIE and the g_i in the cost function are corresponding to each other in order to merge like terms in the subsequent derivation. In addition, if $g_i = 0$, the system needs longer time to achieve the same estimation performance and control performance as $g_i = 1$, which is mainly due to the possibility of failure of the error correction term $Y_{ei}(k)$ when $g_i = 0$.

To ensure the stability of the designed IDMPC method, the following three elements are designed.

1) Terminal Controller: The terminal controller for the i-th MR is designed as follows

$$u_{ei}(k) = -K \hat{\phi}_{ei}(k) - H_1 \hat{f}_{di}(k), \tag{15}$$

where K denotes the terminal feedback gain matrix obtained by the LQR algorithm.

2) Terminal Constraint Set: In order to make the system state enter the stability domain earlier, the following theorem is given.

***Theorem** 2:* Based on the terminal controller (15), if there exists a symmetric matrix $W_3 > 0$ and $h \in (0, 1)$ such that the following optimization problem is solvable

$$\begin{aligned} \min \quad & -\log\left(\det W_3\right) \\ s.t. \quad & \begin{bmatrix} hW_3 & * \\ (A_e - B_e K) W_3 & W_3 \end{bmatrix} \geq 0, \\ & \begin{bmatrix} \frac{1}{\eta \lambda^2} \left(1 - \sqrt{h}\right)^2 I & * \\ HC & W_3 \end{bmatrix} \geq 0, \end{aligned} \tag{16}$$

then a maximum terminal constraint set $E_{tcs} = \left\{ \hat{\phi}_e : \hat{\phi}_e^T \left(I_N \otimes P_3 \right) \hat{\phi}_e \leq 1, P_3 = W_3^{-1} \right\}$ can be obtained.

***Proof*:** Please See the Appendix.B. ■

3) Terminal Penalty Matrix: For $\forall \hat{\phi}_e \in E_{tcs}$, the terminal penalty matrix needs to satisfy the following inequality

$$\begin{aligned} & \hat{\phi}_e^T(k+1) \left(I_N \otimes P_4 \right) \hat{\phi}_e(k+1) - \hat{\phi}_e^T(k) \left(I_N \otimes P_4 \right) \hat{\phi}_e(k) \\ & \quad + \hat{\phi}_e^T(k) \left(I_N \otimes Q \right) \hat{\phi}_e(k) + u_e^T(k) \left(I_N \otimes R \right) u_e(k) \\ & \quad + \hat{\phi}_e^T(k) \left(M^T M \otimes H_2^T H_2 \right) \hat{\phi}_e(k) \leq 0. \end{aligned} \tag{17}$$

To obtain a smaller terminal penalty matrix and expand the feasible range of the subsequent optimization problem, the following theorem is given.

***Theorem** 3:* Based on the terminal controller (15) and terminal constraint set E_{tcs}, if there exists a symmetric matrix $W_4 = P_4^{-1} > 0$, $h \in (0, 1)$ and $\Upsilon = \left(P_3 + Q + \lambda^2 H_2^T H_2 + 2K^T R K + 2\mu\sigma P_3 - \sqrt{h} P_3 \right)^{\frac{1}{2}}$,

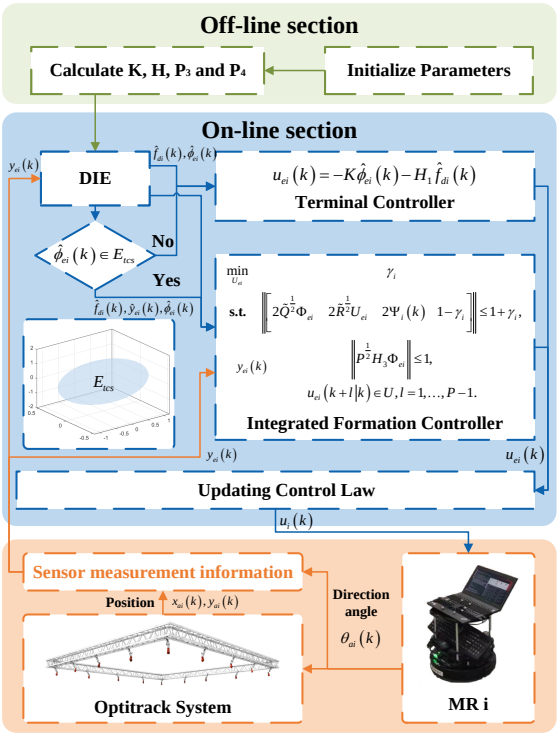

Fig. 3. Block diagram of ADRFC.

then the terminal penalty matrix P_4 can be obtained by solving the following optimization problem

$$\begin{aligned} \min \quad & -\log\left(\det W_4\right) \\ s.t. \quad & \begin{bmatrix} \sqrt{h}W_4 & * & * \\ \left(A_e - B_e K\right)W_4 & W_4 & * \\ \Upsilon W_4 & 0 & \frac{1}{\sqrt{h}} \end{bmatrix} \geq 0, \\ & \begin{bmatrix} \frac{1}{\eta\lambda^2}\left(1-\sqrt{h}\right)^2 & * \\ HC & W_4 \end{bmatrix} \geq 0. \end{aligned} \tag{18}$$

***Proof*:** Please See the Appendix.C. ■

C. Integrated Formation Controller

Combining the previously designed DIE and IDMPC, the integrated formation controller of MAS is constructed, and its structural block diagram is shown in Fig. 3. The control objective of each MR can be described by the following optimization problem

$$\min_{\{u_{ei}(k)\ldots u_{ei}(k+P-1)\}} \quad J_i\left(k\right) \tag{19}$$

s.t.

$$\begin{aligned} \hat{\phi}_{ei}\left(k+l+1\right) &= A_e\hat{\phi}_{ei}\left(k+l\right) + B_e u_{ei}\left(k+l\right) \\ &\quad + B_f\hat{f}_{di}\left(k+l\right) + HY_{ei}\left(k+l\right), \qquad (19a) \\ \hat{y}_{ei}\left(k+l\,|k\right) &= C_e\hat{\phi}_{ei}\left(k+l\,|k\right), \ l=1,\ldots,P, \qquad (19b) \\ u_i\left(k\,|k\right) &= \left[\ v_{ai}\left(k\,|k\right) \quad \omega_{ai}\left(k\,|k\right)\ \right]^T, \\ u_i\left(k+l\,|k\right) &\in U, \ l=1,\ldots,P-1, \qquad (19c) \\ \hat{\phi}_{ei}\left(k+P\,|k\right) &\in E_{tcs}. \qquad (19d) \end{aligned}$$

***Remark** 5:* Equations (19a) and (19b) represent the error state prediction equation and output equation based on the estimated value, and Eqn. (19c) represents the control input constraint. It should be noted that (19c) is the input constraints of the MR, which are obtained through a nonlinear mapping between the VMR and control input u_{ei}. Equation (19d) represents the terminal constraints. It should be highlighted that the state/output feedback control method cannot completely compensate for the disturbance due to the presence of the input constraints, which prolongs the system convergence time. In contrast, the proposed method adopts the design criterion of the maximum terminal constraint set, which reduces the transient time.

Obviously, Eq. (19) is a local optimization problem, but it contains coupling term from the information of neighboring MRs. The Nash optimization strategy in [34] is usually applied to solve such problem. Assuming that the coupling variables from the neighbors are set as the final iteration values, which means that each MR optimizes its cost function to determine its control input. Then, the whole system can converge to a Nash equilibrium. Due to the presence of non-linear constraints (19d) in the optimization problem, it is converted into a second-order cone program (SOCP) problem to solve. According to (10), the prediction equation of IDMPC can be obtained

$$\begin{aligned} \hat{\phi}_{ei}\left(k+1\right) =& A_e\hat{\phi}_{ei}\left(k\right) + B_e u_{ei}\left(k\right) + B_f\hat{f}_{di}\left(k\right) + HY_{ei}\left(k\right), \\ & \vdots \\ \hat{\phi}_{ei}\left(k+P\right) =& A_e^N\hat{\phi}_{ei}\left(k\right) \\ & + A_e^{N-1}B_e u_{ei}\left(k\right)\ldots + B_e u_{ei}\left(k+P-1\right) \\ & + A_e^{N-1}B_f\hat{f}_{di}\left(k\right)\ldots + B_f\hat{f}_{di}\left(k+P-1\right) \\ & + A_e^{N-1}HY_{ei}\left(k\right)\ldots + HY_{ei}\left(k+P-1\right). \end{aligned}$$

Note that $\hat{f}_{di}(k+l)$ and $Y_{ei}(k+l)$ $(l=1,\ldots,P-1)$ represent future disturbance estimation and error correction, while future information is not available. To increase the feasible region of the optimization objective, it is reasonable to assume that the future measurements are equal to the present measurements [32]. It should be noted that, compared to the use of independently designed formation controller and disturbance compensator, the integrated design approach adds a recursive term about the disturbance $\hat{f}_{di}(k)$ to the MPC prediction equation and performs the solution of the control law on this basis. In this case, the resulting control law already integrates the functions of formation control and disturbance rejection. The controller can automatically trade-off formation control and disturbance rejection and can improve the transient performance of the system. Then, it is rewritten into a matrix form

$$\Phi_{ei} = \bar{A}\hat{\phi}_{ei}\left(k\right) + \bar{B}_e U_{ei} + \bar{B}_f\hat{f}_{di}\left(k\right) + \bar{H}Y_{ei}\left(k\right), \tag{20}$$

where $\Phi_{ei} = \left[\phi_{ei}^T\left(k+1\right),\ldots\phi_{ei}^T\left(k+P\right)\right]^T$, $U_{ei} = \left[u_{ei}^T\left(k\right),\ldots u_{ei}^T\left(k+P-1\right)\right]^T$, $\bar{B}_f$ and $\bar{H}$ are similar to $\bar{A}$,

$$\bar{A} = \begin{bmatrix} A_e \\ A_e^2 \\ \vdots \\ A_e^N \end{bmatrix}, \bar{B} = \begin{bmatrix} B_e & & & \\ A_eB_e & B_e & & \\ \vdots & \vdots & \ddots & \\ A_e^{N-1}B_e & A_e^{N-2}B_e & \cdots & B_e \end{bmatrix}.$$

Define $\psi_i(k) = \sum a_{ij} H_2\left(\hat{\phi}_{ej}(k|k) - \hat{\phi}_{ei}(k|k)\right) - g_i H_2 \hat{\phi}_{ei}(k|k)$, $\Psi_i = \left[\psi_i^T(k+1), \ldots, \psi_i^T(k+P)\right]^T$. Thus, the local cost function (14) can be written as

$$\begin{aligned} J_i(k) =& \Phi_{ei}^T \tilde{Q} \Phi_{ei} + U_{ei}^T \tilde{R} U_{ei} + \Psi_i^T \Psi_i \\ &+ \hat{\phi}_{ei}^T(k|k) Q \hat{\phi}_{ei}(k|k) + \psi_i^2(k|k), \end{aligned} \tag{21}$$

where $\tilde{Q} = diag\{I_{P-1} \otimes Q, P\}$, $\tilde{R} = I_P \otimes R$.

It can be seen that $\hat{\phi}_{ei}^T(k|k) Q \hat{\phi}_{ei}(k|k)$ and $\psi_i^2(k|k)$ are independent of the optimization objective U_{ei}. Define γ_i as the upper bound of $J_i(k) - \hat{\phi}_{ei}^T(k|k) Q \hat{\phi}_{ei}(k|k) - (\psi_i(k|k))^2$, one can obtain

$$\Phi_{ei}^T \tilde{Q} \Phi_{ei} + U_{ei}^T \tilde{R} U_{ei} + \Psi_i^T \Psi_i \leq \gamma_i. \tag{22}$$

Further, (22) and the nonlinear constraint (19d) are equivalent to

$$\begin{aligned} 4\Phi_{ei}^T \tilde{Q} \Phi_{ei} + 4U_{ei}^T \tilde{R} U_{ei} + 4\Psi_i^T \Psi_i + (1-\gamma_i)^2 \leq (1+\gamma_i)^2, \\ \Phi_{ei}^T H_3^T P H_3 \Phi_{ei} \leq 1. \end{aligned} \tag{23}$$

where $H_3 = [\underbrace{0 \quad \ldots \quad 0}_{P-1} \quad I]$. Combining (23) and (19c), the final SOCP optimization problem can be described

$$\begin{aligned} \min_{U_{ei}} \quad & \gamma_i \\ \text{s.t.} \quad & \left\| \begin{bmatrix} 2\tilde{Q}^{\frac{1}{2}} \Phi_{ei} & 2\tilde{R}^{\frac{1}{2}} U_{ei} & 2\Psi_i(k) & 1-\gamma_i \end{bmatrix} \right\| \leq 1+\gamma_i, \\ & \left\| P^{\frac{1}{2}} H_3 \Phi_{ei} \right\| \leq 1, \\ & u_{ei}(k+l|k) \in U, l = 1, \ldots, P-1. \end{aligned} \tag{24}$$

If the above optimization problem is solvable, then the first optimal control sequence $u_{ei}^*(k) = [\, I \quad \underbrace{0 \quad \ldots \quad 0}_{P-1} \,] U_{ei}^*$ is extracted. According to $u_{ei}^* = \begin{bmatrix} v_{vi}\cos\hat{\theta}_{ei} - v_{ai}(k) & \omega_{vi} - \omega_{ai} \end{bmatrix}^{\mathrm{T}}$, the final integrated formation controller of each MR is obtained. The proposed ADRFC is summarized in Algorithm 1.

Remark 6: Since the optimization problem considered in this paper has a terminal constraint $\hat{\phi}_{ei}(k+P|k) \in E_{tcs}$ in the form of an L_2 norm, which cannot be solved using the QP or QCQP algorithms. Therefore, it is transformed into a more generalized SOCP problem and solved quickly using an advanced Mosek solver. Note that either QP or QCQP is a special case of the SOCP problem.

In Algorithm 1, all the parameters can be categorized into experimental parameters (ϕ_{vi}, $\hat{\phi}_{ei}$, v_{vi}, ω_{vi}, θ_{ij}^r) and algorithmic parameters (ε, h, ϖ, θ_{ij}^r, κ, Q, R, P). In the experimental parameters, ϕ_{vi}, v_{vi} and ω_{vi} mean the state information, linear velocity, and angular velocity of the VMR, respectively. $\hat{\phi}_{ei}$ denotes the estimated initial value of the tracking error, and θ_{ij}^r represents the desired formation angular difference. The above parameters are those that need to be set in advance in the experiment and will not affect the performance of the algorithm. Among the algorithm parameters, ε, h, ϖ, κ, q_{max}, Q, R and P are the parameter settings regarding DIE and IDMPC, where ε and h are the parameters in (13), (16) and (18), which are only needed to ensure that the LMI is solvable.

Algorithm 1 ADRFC Controller Design Method

Off-line section:

1: Given the initial parameter ϕ_{vi}, $\hat{\phi}_{ei}$, v_{vi}, ω_{vi}, ε, h, ϖ, θ_{ij}^r, κ, Q, R and P. Set $u_{ei} = 0$, the number of iteration $q = 0$, and the maximum number of iteration q_{max}.

2: Calculate terminal controller gain K. Solve optimization problems (13), (16) and (18) to obtain H, E_{tcs} and P_4.

On-line section:

3: Using DIE to obtain information about $\hat{\phi}_{ei}(k)$ and $\hat{f}_{di}(k)$.

4: According to the communication topology, the MR i exchange $\hat{\phi}_{ei}(k)$ and $u_{ei}^q(k)$ between its neighbors.

5: If $q \leq q_{max}$ and $\hat{\phi}_{ei}(k) \in E_{tcs}$, $u_{ei}^{p+1}(k) = -K\hat{\phi}_{ei}(k) - H_1 \hat{f}_{di}(k)$; If $q \leq q_{max}$ and $\hat{\phi}_{ei}(k) \notin E_{tcs}$, solve the SOCP optimization problem to obtain $u_{ei}^{q+1}(k)$; If $q > q_{max}$, stop the iteration, go to Step 7.

6: If all MRs meet the stopping criteria

$$\left\| u_{ei}^{q+1}(k) - u_{ei}^q(k) \right\| \leq \kappa$$

then stop the iteration, set $u_{ei}(k) = u_{ei}^q(k)$. Otherwise, let $q = q+1$, go to Step 4.

7: Based on $u_{ei} = \begin{bmatrix} v_{vi}\cos\hat{\theta}_{ei} - v_{ai} & \omega_{vi} - \omega_{ai} \end{bmatrix}^T$, $v_{ai}(k)$ and $\omega_{ai}(k)$ are obtained and applied to the MR i. Set $q = 0$, $k = k+1$, go to Step 3.

ϖ is a tuning parameter of the DIE, which is mainly adjusted according to the estimation performance and overshooting. κ and q_{max} denote the expected difference of the control law and the maximum number of iterations of Nash equilibrium. Under the premise of ensuring that the single iteration time of the algorithm is within the sampling time, κ should be as small as possible and q_{max} should be as large as possible. Q and R represent the weighting coefficients of IDMPC, which indicate the emphasis on the system state and controller, respectively. P represents the prediction horizon of IDMPC. All the above algorithm parameters need to be adjusted according to the actual experimental situation, the only principle is that the single iteration time of the algorithm must be guaranteed to be within the sampling time.

The specific logic of the algorithm is as follows. First, some of the initial parameters are given in the offline phase and the terminal controller gain, DIE observer gain, terminal constraint set and terminal penalty matrix are calculated. Then, the mobile robot is placed in the experimental site to start running, and the algorithm first obtains an estimate about the tracking error state and disturbance by DIE, and then a set of control laws are obtained by IDMPC. Next, a Nash optimization strategy is used to continuously optimize the control laws until the before and after control law errors are within the desired range. Finally, the final control law for each mobile robot is inversely solved and applied to the robot, thus realizing active disturbance rejection formation control.

D. Stability Analysis

After completing the design of the IMPC and the controller, the main result is given as the following theorem.

Theorem 4: If the optimization problem (24) has a solution at the moment $k = 0$, then its optimization problem is feasible

for any $k > 0$ moments, and the closed-loop system consisting of Algorithm 1 is asymptotically stable.

***Proof*:** Suppose that by solving the SOCP optimization problem at moment k, the optimal control sequence is $U_e^*(k) = \{u_e^*(k\,|k), \ldots, u_e^*(k+P-1\,|k)\}$, and its corresponding state sequence is $\left\{\hat{\phi}_e^*(k+1\,|k), \ldots, \hat{\phi}_e^*(k+P\,|k)\right\}$, both of them satisfy control and terminal constraint, where $u_e^* = [u_{e1}^{*T}, ..., u_{eN}^{*T}]^T$ and $\phi_e^* = [\hat{\phi}_{e1}^{*T}, ..., \hat{\phi}_{eN}^{*T}]^T$. Then, the global optimal cost function $J^*(k)$ can be expressed as:

$$\begin{aligned} J^*(k) = \sum_{l=0}^{P-1} (& \left\|\hat{\phi}_e^*(k+l\,|k)\right\|^2_{(I_N\otimes Q)} + \|u_e^*(k+l\,|k)\|^2_{(I_N\otimes R)} \\ & + \left\|\hat{\phi}_e^*(k+l\,|k)\right\|^2_{\left(M^TM\otimes H_2^TH_2\right)}) \\ & + \left\|\hat{\phi}_e^*(k+P\,|k)\right\|^2_{(I_N\otimes P_4)}. \end{aligned} \tag{25}$$

To obtain an admissible control sequence $U_e(k+1)$ for optimization problem at time $k+1$, take the control sequence to be $U_e(k+1) = \{u_e^*(k+1\,|k), \ldots, u_e^*(k+P-1\,|k), u_e^*(k+P\,|k)\}$, where $u_e^*(k+P\,|k) = -(I_N\otimes K)\hat{\phi}_e^*(k+P\,|k) - (I_N\otimes H_1)\hat{f}_d(k)$. Then, according (25) and $U_e(k+1)$, it is not difficult to conclude that

$$\begin{aligned} J(k+1) = & J^*(k) - \left\|\hat{\phi}_e^*(k\,|k)\right\|^2_{(I_N\otimes Q)} - \|u_e^*(k\,|k)\|^2_{(I_N\otimes R)} \\ & - \left\|\hat{\phi}_e^*(k\,|k)\right\|^2_{\left(M^TM\otimes H_2^TH_2\right)} \\ & + \left\|\hat{\phi}_e^*(k+P+1\,|k)\right\|^2_{(I_N\otimes P_4)} \\ & + \|u_e^*(k+P\,|k)\|^2_{(I_N\otimes R)} \\ & + \left\|\hat{\phi}_e^*(k+P\,|k)\right\|^2_{\left(M^TM\otimes H_2^TH_2\right)} \\ & - \left\|\hat{\phi}_e^*(k+P\,|k)\right\|^2_{(I_N\otimes P_4)} \\ & + \left\|\hat{\phi}_e^*(k+P\,|k)\right\|^2_{(I_N\otimes Q)}. \end{aligned} \tag{26}$$

From the properties of $\hat{\phi}_{ei}^*(k+P\,|k) \in E_{tcs}$ (17) and the terminal penalty matrix P_4, one can conclude that $U_e(k+1)$ satisfies the controller constraints (19c) and the system satisfies the terminal constraints (19d). Thus, the control sequence $U_e(k+1)$ at moment $k+1$ is a feasible solution to the optimization problem (24), and the following inequality can be derived

$$\begin{aligned} J(k+1) \leq & J^*(k) - \left\|\hat{\phi}_e^*(k\,|k)\right\|^2_{(I_N\otimes Q)} - \|u_e^*(k\,|k)\|^2_{(I_N\otimes R)} \\ & - \left\|\hat{\phi}_e^*(k\,|k)\right\|^2_{\left(M^TM\otimes H_2^TH_2\right)}. \end{aligned} \tag{27}$$

Since $\hat{\phi}_e^*(k\,|k) = \hat{\phi}_e(k\,|k)$, $u_e^*(k\,|k) = u_e(k\,|k)$. If there is an optimal solution to the optimization problem at instant $k+1$, then it can be obtained

$$\begin{aligned} J^*(k+1) \leq & J(k+1) \leq J^*(k) - \left\|\hat{\phi}_e^*(k\,|k)\right\|^2_{(I_N\otimes Q)} \\ & - \left\|\hat{\phi}_e^*(k\,|k)\right\|^2_{\left(M^TM\otimes H_2^TH_2\right)}. \end{aligned} \tag{28}$$

Therefore, $J^*(k)$ can be regarded as a Lyapunov function for a closed-loop system that is nominally asymptotically stable. This completes the stability proof. ■

IV. Experimental Verification

In this section, experiments will be conducted on the previously mentioned mobile robot experimental platform to verify the effectiveness and superiority of the ADRFC method. The adopted formation is shown in Fig. 2, the radius of the circular trajectory is 2 m. The sampling time of the whole system is set to 0.05s. The computer configuration for executing the program is as follows: Intel Core i5-7300HQ, 16GB RAM, MATLAB R2022a, Ubuntu 18.04, ROS Melodic. Through the publisher and subscriber, real-time communication between MATLAB and ROS is performed so as to complete command sending and data uploading.

A. Formation Control Experiment

In this subsection, formation control experiments are performed to verify the effectiveness of ADRFC via the experimental platform as shown in Fig. 1, and the desired formation is presented in Fig. 2. The reference angular velocity $\omega_{vi} = \frac{2\pi}{25} rad/s$, the reference linear velocity $v_{vi} = \frac{4\pi}{25} m/s$, and the reference angular difference $\theta_{12}^r = \theta_{23}^r = \theta_{34}^r = \frac{\pi}{4}$. The initial parameters of each VMR are set as follows: $\phi_{v1}(k) = \begin{bmatrix} 1-\sqrt{2} & 1+\sqrt{2} & \frac{5\pi}{4} \end{bmatrix}^{\mathrm{T}}$, $\phi_{v2}(k) = \begin{bmatrix} 1 & 3 & \pi \end{bmatrix}^{\mathrm{T}}$, $\phi_{v3}(k) = \begin{bmatrix} 1+\sqrt{2} & 1+\sqrt{2} & \frac{3\pi}{4} \end{bmatrix}^{\mathrm{T}}$, $\phi_{v4}(k) = \begin{bmatrix} 3 & 1 & \frac{\pi}{2} \end{bmatrix}^{\mathrm{T}}$. Set the disturbance for each MR as follows

$$\begin{cases} f_{d1}(k) = & 0.2, & k > 50 \\ f_{d2}(k) = & -0.3, & k > 100 \\ f_{d3}(k) = & 0.25\sin\left(\frac{\pi k}{75}\right), & k > 75 \\ f_{d4}(k) = & 0.3\cos\left(\frac{\pi k}{100}\right), & k > 150 \end{cases}$$

The DIE parameter $\varpi = 70$, and the IDMPC parameters are given as $P = 8$, $Q = diag(5000, 5000, 100)$, $R = 20I$, $h = 0.99$, $\kappa = 0.01$, $\eta = 1$, $\mu = 0.5$, $q_{max} = 20$, $\varepsilon = 1$, $\begin{bmatrix} -0.5487 & -0.4743 \end{bmatrix}^{\mathrm{T}} \leq U \leq \begin{bmatrix} 0.6513 & 0.6257 \end{bmatrix}^{\mathrm{T}}$. The matrices solved from the linear matrix inequalities are as follows

$$K = \begin{bmatrix} 10.7664 & -1.1841 & -0.0906 \\ -0.1636 & 14.1103 & 3.9854 \end{bmatrix},$$

$$H = \begin{bmatrix} 0.2048 & 0.0026 & 0 \\ -0.0026 & 0.2048 & 0.0051 \\ 0 & 0 & 0.2238 \end{bmatrix},$$

$$W_3 = \begin{bmatrix} 1.3878 & 0.0545 & -0.0543 \\ 0.0545 & 0.2894 & -0.3853 \\ -0.0543 & -0.3853 & 2.4933 \end{bmatrix},$$

$$W_4 = \begin{bmatrix} 0.0314 & 0.0058 & 0.0106 \\ 0.0058 & 0.0109 & 0.0122 \\ 0.0106 & 0.0122 & 0.0870 \end{bmatrix}.$$

The trajectory diagram of the MRs under the ADRFC method is displayed in Fig. 4, and the results show that the four MRs can accurately track the trajectories generated by the VMRs and form a desired formation. In addition, since

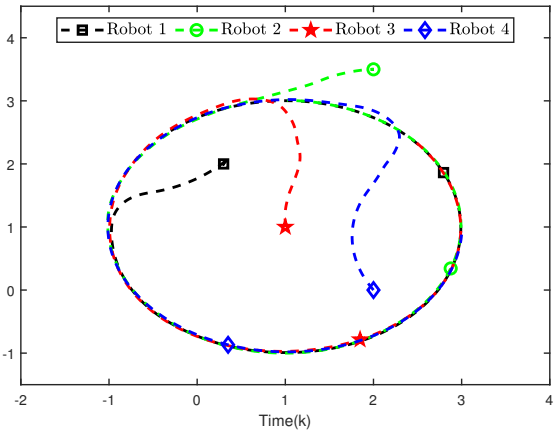

Fig. 4. Experimental trajectories of four MRs (Unit: m).

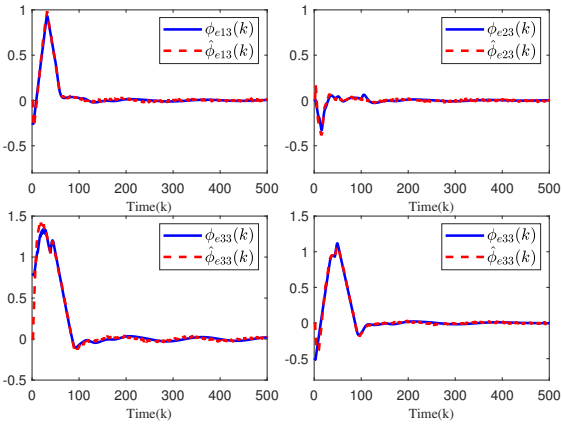

Fig. 5. Experimental results of error state $\phi_{ei3}(k)$ and its estimation $\hat{\phi}_{ei3}(k)$ (Unit: m)

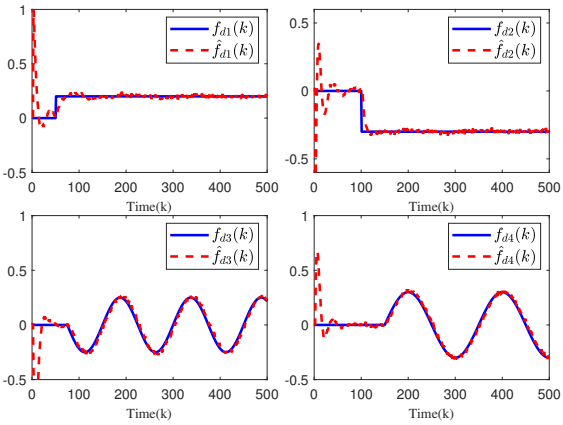

Fig. 6. Experimental results of disturbance $f_{di}(k)$ and its estimation $\hat{f}_{di}(k)$ (Unit: m).

the disturbances occur in the directional angles of the MRs, the curves of error state $\phi_{ei3}(k)$ and their estimation results are presented in Fig. 5. The results show that after a short period of oscillation, the ADRFC is able to accurately estimate the error state of each MR and ensure its convergence, thus enabling the MR to complete the corresponding path tracking task. Meanwhile, the directional angle error states of the four MRs fluctuate at 50, 75, 100 and 150 steps, which correspond to the time when the disturbances occur. Then, the proposed ADRFC can obtain accurate disturbances estimation results (as shown in Fig. 6) and adjust automatically, which makes the error states of the MRs recover quickly. Further, the

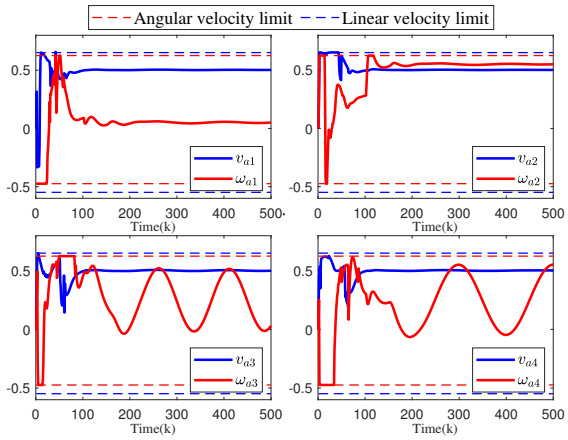

Fig. 7. Mobile robot linear velocity v_{ai}, angular velocity ω_{ai} and limits.

linear and angular velocity control laws for the four mobile robots are given in Fig. 7. Therein, the blue dashed line and the red dashed line indicate the limits of linear and angular velocities, respectively, the blue solid line and the red solid line represent the actual control laws. It can be seen that the linear and angular velocities of each mobile robot are strictly limited to the upper and lower bound regions. Meanwhile, since the disturbance occurs in the angular velocity, the linear velocity control law is eventually stabilized around $\frac{4\pi}{25}$, while the angular velocity control law is adjusted according to the disturbance, showing a constant shift or a sinusoidal shift. The above experimental results demonstrate that the ADRFC can obtain accurate error state and disturbance estimation information, and can effectively perform the path tracking task and formation control task of the MAS under the dual influence of input constraints and disturbances.

B. Comparison Experiment

TABLE I
COMPARISON METHODS

Method	Observer	Controller	Disturbance rejection
ADRFC	DIE	IDMPC	INT
CM1	DIE	IDMPC	INT
CM2 [21]	DIE	FB	IND
CM3 [15]	ESO	FB	IND
CM4	DIE	IDMPC	IND
CM5 [35]	ESO	IDMPC	IND
CM6	DIE	IDMPC	INT

Furthermore, to highlight the superiority of the ADRFC method, comparison experiments are conducted with the common methods listed in Table. I. In Table I, the observer, controller, and design ideas of disturbance rejection adopted by different methods are presented, where ESO denotes the widely used extended state observer [14], [15], [35]; FB is the state feedback controller; DR and NDR represent the approaches with and without disturbance rejection, respectively; INT and IND indicate the relationship between the formation controller and disturbance rejection, INT means that the disturbance rejection is integrated into the formation controller, and IND shows that the disturbance rejection and

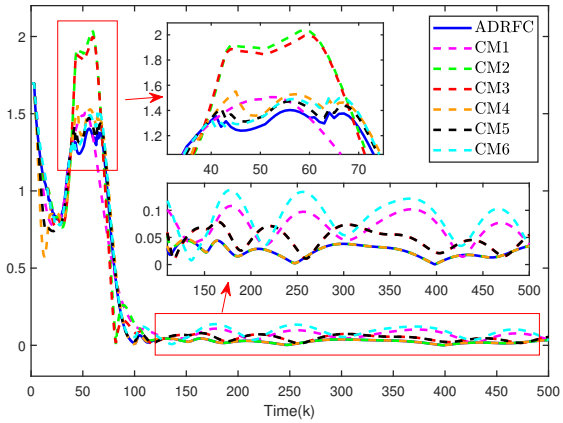

Fig. 8. Experimental formation error E_f.

TABLE II
PERFORMANCE COMPARISON RESULTS

Method	Transient peak	Convergence time (k)	Steady-state peak
ADRFC	**1.403**	**92**	**0.044**
CM1	1.506(6.8%)	119(22.7%)	0.108(59.3%)
CM2	2.040(31.2%)	108(14.8%)	0.044(0%)
CM3	1.999(29.8%)	108(14.8%)	0.079(44.3%)
CM4	1.554(9.7%)	92(0%)	0.045(2.2%)
CM5	1.473(4.8%)	107(14%)	0.079(44.3%)
CM6	1.506(6.8%)	118(22%)	0.137(67.9%)

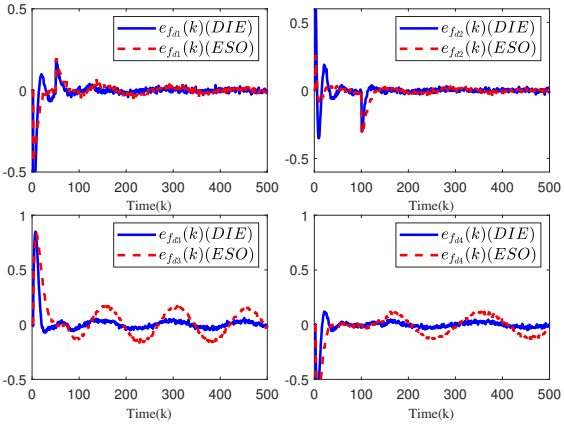

Fig. 9. Experimental results of disturbance estimation error $e_{f_{di}}(k) = f_{di}(k) - \hat{f}_{di}(k)$.

the formation controller are independent of each other. The adjustable parameters ϖ and the observer gain H are the same for the DIE method, and the observer gain is the same for the ESO method. The parameters are equal for the IDMPC methods, the terminal controller gain K and the feedback control gain are the same. CM1 indicates that the maximum terminal constraint set and the minimum terminal penalty are not applied. Additionally, the input constraints are identical for all methods. Since the error in X, Y direction can be represented by the angular error, the total formation error is defined as follows

$$E_f = \sqrt{\sum_{i=1}^{N} \left(\sum_{j \in \mathcal{N}_i} a_{ij} \left| \theta_i(k) - \theta_j(k) - \theta_{ij}^r \right| \right)^2}.$$

Fig. 8 shows the comparison results of the formation errors E_f of the seven methods. To illustrate more clearly the superiority of ADRFC, the specific performances of the seven methods are listed in Table. II, where the percentage performance improvement of ADRFC compared to the methods is indicated in parentheses. It can be seen that ADRFC has the best transient and steady-state performance among all methods, converging at about 92 steps, and its transient and steady-state peaks are only 1.403 and 0.044, respectively. In contrast, the performance of the ADRFC without the maximum terminal constraint set and minimum terminal penalty matrix ('CM1') is degraded, mainly because its stability domain is too small resulting in the system cannot enter the terminal controller action range, thus requiring more time to ensure system convergence. For the 'CM2' and 'CM3' with state feedback control, it is found that their transient peaks are the highest and their convergence speed is inferior to the ADRFC due to the presence of input constraints. In addition, the different steady-state peaks of the two methods are mainly due to the significant errors in the estimation of the error states and disturbances by ESO. As shown in Fig. 9, the estimation error of DIE and ESO for the disturbance is demonstrated $e_{f_{di}}(k) = f_{di}(k) - \hat{f}_{di}(k)$, where $f_{di}(k)$ denotes the actual value of the disturbance and $\hat{f}_{di}$ represents the estimated value of the disturbance. It can be seen that the estimation performance of ESO for disturbances is significantly inferior to DIE. The transient peaks of both 'CM4' and 'CM5' with IDMPC control are effectively reduced compared to the state feedback control method, and the convergence time of 'CM4' is also improved. However, the disturbance rejection and the formation controller of the above four methods are independent of each other, and the

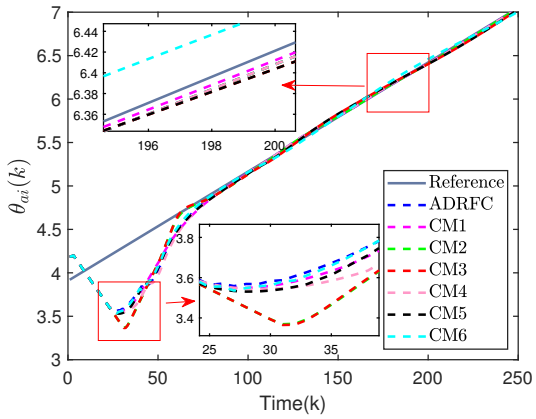

Fig. 10. Mobile robot state θ_{a1} curve.

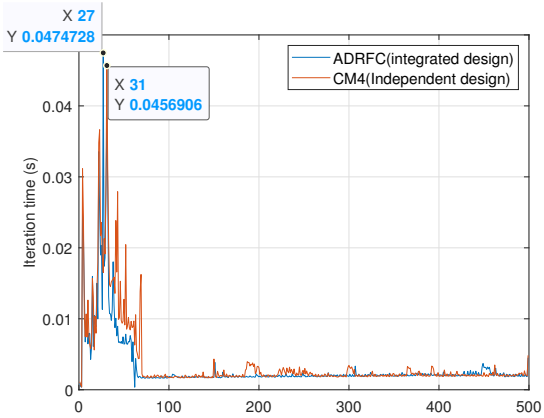

Fig. 11. Iteration time for ADRFC and CM4

ADRFC adopts the idea of integrated design, which makes the ADRFC surpass the above methods in all performance metrics. The last one, 'CM6', is a special case of ADRFC without disturbance rejection, which has the highest steady-state peak among all the approaches and its convergence time is longer due to disturbance. In addition, since the disturbance occurs on the angular velocity controller, the direction angle curves of MR1 θ_{a1} under different methods are given, as shown in Fig. 10. From the figure, it can be seen that among all the compared methods, the state curve of ADRFC has the smallest amount of overshooting within 10-50 steps and can quickly and smoothly converge to the reference value. In contrast, the overshooting of CM3, CM2, CM4, CM5, CM1, and CM6 decreases in order. And after entering the steady state, the steady state error of CM6 is the largest because it does not suppress the disturbance, while the steady state errors of the remaining methods are relatively close to each other, all within 0.01. Among the six comparison methods mentioned above, CM4 is the closest method to ADRFC, and the main difference is that CM4 adopts the independent design idea, while ADRFC utilizes the integrated design approach. In order to distinguish the two approaches more clearly, the iteration time images of both are given in Fig. 11. Combining Table II and Fig. 11, it can be obtained that ADRFC reduces the overshoot by 10% at the expense of 3.9% iteration time. It is worth noting that in some practical trajectory tracking tasks, 10% overshooting can lead to an error of 10cm-20cm, and this error may lead to collision accidents between devices and economic losses. And the ADRFC method can effectively reduce the overshoot within the allowed computation time, which is also applicable to these situations. In summary, this experimental result verifies the effectiveness and superiority of the ADRFC approach in MAS formation control tasks with input constraints and disturbances.

V. Conclusion

This paper provides an ADRFC approach for the formation control task of MAS under input constraints and disturbances. Accurate error state estimation and disturbance estimation can be obtained by DIE. Moreover, an IDMPC method is proposed with a rigorous theoretical proof. In contrast to most existing methods, the disturbance rejection technique is incorporated into the design process of the formation controller and the design criteria of maximum terminal constraint set and minimum terminal penalty matrix are adopted. These improvements allow the controller to perform the path tracking and formation synchronization tasks of the MAS under input constraints and disturbances. Finally, the effectiveness and superiority of the proposed method are demonstrated on a MAS experimental platform.

References

[1] C. Deng and C. Wen, "Distributed resilient observer-based fault-tolerant control for heterogeneous multiagent systems under actuator faults and dos attacks," *IEEE Transactions on Control of Network Systems*, vol. 7, no. 3, pp. 1308–1318, 2020.

[2] C. Liu, B. Jiang, R. J. Patton, and K. Zhang, "Hierarchical-structure-based fault estimation and fault-tolerant control for multiagent systems," *IEEE Transactions on Control of Network Systems*, vol. 6, no. 2, pp. 586–597, 2019.

[3] T. Czimmermann, M. Chiurazzi, and M. Milazzo, "An autonomous robotic platform for manipulation and inspection of metallic surfaces in industry 4.0," *IEEE Transactions on Automation Science and Engineering*, vol. 19, no. 3, pp. 1691–1706, 2022.

[4] M. Dotoli, H. Zgaya, C. Russo, and S. Hammadi, "A multi-agent advanced traveler information system for optimal trip planning in a co-modal framework," *IEEE Transactions on Intelligent Transportation Systems*, vol. 18, no. 9, pp. 2397–2412, 2017.

[5] P. Ghassemi and S. Chowdhury, "Multi-robot task allocation in disaster response: Addressing dynamic tasks with deadlines and robots with range and payload constraints," *Robotics and Autonomous Systems*, vol. 147, p. 103905, 2022.

[6] G. Wen, X. Fang, J. Zhou, and J. Zhou, "Robust formation tracking of multiple autonomous surface vessels with individual objectives: A noncooperative game-based approach," *Control Engineering Practice*, vol. 119, p. 104975, 2022.

[7] X. Wang, S. Li, X. Yu, and J. Yang, "Distributed active anti-disturbance consensus for leader-follower higher-order multi-agent systems with mismatched disturbances," *IEEE Transactions on Automatic Control*, vol. 62, no. 11, pp. 5795–5801, 2017.

[8] W. Cheng, K. Zhang, B. Jiang, and S. X. Ding, "Fixed-time fault-tolerant formation control for heterogeneous multi-agent systems with parameter uncertainties and disturbances," *IEEE Transactions on Circuits and Systems I: Regular Papers*, vol. 68, no. 5, pp. 2121–2133, 2021.

[9] S. Chen, H. Pei, Q. Lai, and H. Yan, "Multitarget tracking control for coupled heterogeneous inertial agents systems based on flocking behavior," *IEEE Transactions on Systems, Man, and Cybernetics: Systems*, vol. 49, no. 12, pp. 2605–2611, 2019.

[10] X. Wu, G. Huang, F. Guo, Q. Lu, J. She, and L. Yu, "An adaptive filter-based equivalent-input-disturbance approach for networked control systems with measurement noise," *IEEE Transactions on Industrial Electronics*, vol. 70, no. 6, pp. 6170–6179, 2023.

[11] J. Zhang, D. Chen, G. Shen, Z. Sun, and Y. Xia, "Disturbance observer based adaptive fuzzy sliding mode control: A dynamic sliding surface approach," *Automatica*, vol. 129, p. 109606, 2021.

[12] X. Yao and L. Guo, "Composite anti-disturbance control for markovian jump nonlinear systems via disturbance observer," *Automatica*, vol. 49, no. 8, pp. 2538–2545, 2013.

[13] D. Yan, W. Zhang, H. Chen, and J. Shi, "Robust control strategy for multi-uavs system using mpc combined with kalman-consensus filter and disturbance observer," *ISA Transactions*, vol. 135, pp. 35–51, 2023.

[14] Q. Wu, L. Yu, Y.-W. Wang, and W.-A. Zhang, "Leso-based position synchronization control for networked multi-axis servo systems with time-varying delay," *IEEE/CAA Journal of Automatica Sinica*, vol. 7, no. 4, pp. 1116–1123, 2020.

[15] X. Wu, Q. Lu, J. She, M. Sun, L. Yu, and C.-Y. Su, "On convergence of extended state observers for nonlinear systems with non-differentiable uncertainties," *ISA Transactions*, 2022.

[16] Y. Wang, Y. Yuan, and J. Liu, "Finite-time leader-following output consensus for multi-agent systems via extended state observer," *Automatica*, vol. 124, p. 109133, 2021.

[17] Y.-W. Wang, W.-A. Zhang, and L. Yu, "A linear active disturbance rejection control approach to position synchronization control for networked interconnected motion system," *IEEE Transactions on Control of Network Systems*, vol. 7, no. 4, pp. 1746–1756, 2020.

[18] J.-H. She, M. Fang, Y. Ohyama, H. Hashimoto, and M. Wu, "Improving disturbance-rejection performance based on an equivalent-input-disturbance approach," *IEEE Transactions on Industrial Electronics*, vol. 55, no. 1, pp. 380–389, 2008.

[19] X. Wu, J. She, L. Yu, H. Dong, and W.-A. Zhang, "Contour tracking control of networked motion control system using improved equivalent-input-disturbance approach," *IEEE Transactions on Industrial Electronics*, vol. 68, no. 6, pp. 5155–5165, 2021.

[20] J.-W. Zhu, G.-H. Yang, H. Wang, and F. Wang, "Fault estimation for a class of nonlinear systems based on intermediate estimator," *IEEE Transactions on Automatic Control*, vol. 61, no. 9, pp. 2518–2524, 2016.

[21] J.-W. Zhu, G.-H. Yang, W.-A. Zhang, and L. Yu, "Cooperative fault tolerant tracking control for multiagent systems: An intermediate estimator-based approach," *IEEE Transactions on Cybernetics*, vol. 48, no. 10, pp. 2972–2980, 2018.

[22] J.-W. Zhu, C.-Y. Gu, S. X. Ding, W.-A. Zhang, X. Wang, and L. Yu, "A new observer-based cooperative fault-tolerant tracking control method with application to networked multiaxis motion control system," *IEEE Transactions on Industrial Electronics*, vol. 68, no. 8, pp. 7422–7432, 2021.

[23] M. Rosenfelder, H. Ebel, and P. Eberhard, "Cooperative distributed nonlinear model predictive control of a formation of differentially-driven

mobile robots," *Robotics and Autonomous Systems*, vol. 150, p. 103993, 2022.
[24] R. Zhao, M. Miao, J. Lu, Y. Wang, and D. Li, "Formation control of multiple underwater robots based on admm distributed model predictive control," *Ocean Engineering*, vol. 257, p. 111585, 2022.
[25] D. Zhao, D. Liu, and L. Liu, "Distributed and privacy preserving mpc with global constraints over time-varying communication," *IEEE Transactions on Control of Network Systems*, pp. 1–11, 2022.
[26] F. Gavilan, R. Vazquez, and E. F. Camacho, "Chance-constrained model predictive control for spacecraft rendezvous with disturbance estimation," *Control Engineering Practice*, vol. 20, no. 2, pp. 111–122, 2012.
[27] A. Liu, W.-A. Zhang, L. Yu, H. Yan, and R. Zhang, "Formation control of multiple mobile robots incorporating an extended state observer and distributed model predictive approach," *IEEE Transactions on Systems, Man, and Cybernetics: Systems*, vol. 50, no. 11, pp. 4587–4597, 2020.
[28] S. Lin, R. Jia, M. Yue, and Y. Xu, "On composite leader-follower formation control for wheeled mobile robots with adaptive disturbance rejection," *Applied Artificial Intelligence*, vol. 33, no. 14, pp. 1306–1326, 2019.
[29] H. Xie, L. Dai, Y. Lu, and Y. Xia, "Disturbance rejection mpc framework for input-affine nonlinear systems," *IEEE Transactions on Automatic Control*, vol. 67, no. 12, pp. 6595–6610, 2022.
[30] B. Xu, H.-T. Zhang, H. Meng, B. Hu, D. Chen, and G. Chen, "Moving target surrounding control of linear multiagent systems with input saturation," *IEEE Transactions on Systems, Man, and Cybernetics: Systems*, vol. 52, no. 3, pp. 1705–1715, 2022.
[31] H. Zhang, L. Dou, B. Xin, J. Chen, M. Gan, and Y. Ding, "Data collection task planning of a fixed-wing unmanned aerial vehicle in forest fire monitoring," *IEEE Access*, vol. 9, pp. 109 847–109 864, 2021.
[32] D. Qin, A. Liu, J. Xu, W.-A. Zhang, and L. Yu, "Learning from human demonstrations for wheel mobile manipulator: An unscented model predictive control approach," *IEEE Transactions on Neural Networks and Learning Systems*, pp. 1–11, 2022.
[33] H. Wei, Q. Sun, J. Chen, and Y. Shi, "Robust distributed model predictive platooning control for heterogeneous autonomous surface vehicles," *Control Engineering Practice*, vol. 107, p. 104655, 2021.
[34] Y. Zhang and S. Li, "Networked model predictive control based on neighbourhood optimization for serially connected large-scale processes," *Journal of Process Control*, vol. 17, no. 1, pp. 37–50, 2007.
[35] A. Liu, R. Zhang, W.-A. Zhang, and Y. Teng, "Nash-optimization distributed model predictive control for multi mobile robots formation," *Peer-to-Peer Networking and Applications*, vol. 10, no. 3, pp. 688–696, 2017.
[36] Y. Wang, L. Xie, and C. E. Souza, "Robust control of a class of uncertain nonlinear systems," *Systems & Control Letters*, vol. 19, no. 2, pp. 139–149, 1992.

APPENDIX

A. Proof of Theorem 1

Consider the Lyapunov function as

$$V(k) = e_\phi^T(k)(I_N \otimes P_1)e_\phi(k) + e_\varepsilon^T(k)(I_N \otimes P_2)e_\varepsilon(k) \tag{29}$$

Based on (11)-(12), (29) and Young's inequality [36], denote an augmented vector $e = \begin{bmatrix} e_\phi^T & e_\delta^T \end{bmatrix}^T$, one knows

$$\Delta V(k) \le e^T(k)\Pi e(k) + (I_N \otimes (P_2 + 2\varepsilon))\theta_f^2 \tag{30}$$

where $\Pi = \begin{bmatrix} \Pi_{11} & \Pi_{12} \\ * & \Pi_{22} \end{bmatrix}$, and

$$\begin{aligned}\Pi_{11} =& \left(I_N \otimes A_1^T P_1 A_1\right) - 2\left(M \otimes A_1^T P_1 LC\right) \\ &+ \left(M^T M \otimes C^T L^T P_1 LC\right) - \left(I_N \otimes A_2^T P_2 A_2\right) \\ &- (I_N \otimes P_1) + \frac{1}{\varepsilon}\left(I_N \otimes A_2^T P_2 P_2 A_2\right) \\ \Pi_{12} =& \left(I_N \otimes A_1^T P_1 B_f\right) - \left(M \otimes C^T L^T P_1 B_f\right) \\ &+ \left(I_N \otimes A_2^T P_2 A_3\right) \\ \Pi_{22} =& \left(I_N \otimes B_f^T P_1 B_f\right) + \left(I_N \otimes A_3^T P_2 A_3\right) \\ &+ \frac{1}{\varepsilon}\left(I_N \otimes A_3^T P_2 P_2 A_3\right) - (I_N \otimes P_2)\end{aligned}$$

Denote $\Pi_o = -\Pi$, if $\Pi < 0$, i.e., $\Pi_o > 0$, it can be concluded from (30) that

$$\Delta V(k) \le -\alpha V(k) + \beta,$$

where $\alpha = \frac{\lambda_{\min}(-\Pi_o)}{\max[\lambda_{\max}(P_1), \lambda_{\max}(P_2)]}$ and $\beta = (\lambda_{\max}(P_2) + 2\varepsilon)\theta_f^2$. Define a set W as follows

$$\begin{aligned}W = \{&(e_\phi(k), e_\delta(k)) \,|\lambda_{\min}(P_1)\|e_\phi(k)\| \\ &+\lambda_{\min}(P_2)\|e_\delta(k)\| \le \frac{\beta}{\alpha}\Big\}\end{aligned}$$

Let W_s be the supplementary set of W, if $(e_\phi(k), e_\delta(k)) \in W_s$, it follows that

$$V(k) \ge \lambda_{\min}(P_1)\|e_\phi(k)\|^2 + \lambda_{\min}(P_2)\|e_\delta(k)\|^2 \ge \frac{\beta}{\alpha} \tag{31}$$

Combining (30) and (31), if $(e_\phi(k), e_\delta(k)) \in W_s$, one can conclude that

$$\Delta V(k) \le 0$$

Through the Lyapunov theorem, the $(e_\phi(k), e_\delta(k))$ is uniformly ultimately bounded and converges exponentially to W at a rate greater than $e^{-\alpha k}$. Further, by applying the schur complement formula and the spectral decomposition, one obtains that $\Pi < 0$ is equivalent to (13). This completes the proof.

B. Proof of Theorem 2

Substituting the terminal controller into (10), the entire closed-loop system dynamics can be described as

$$\hat{\phi}_e(k+1) = (I_N \otimes (A_e - B_e K))\hat{\phi}_e(k) + (M \otimes HC)e_\phi(k), \tag{32}$$

where $\hat{\phi}_e(k)$ is defined similarly to $e_\phi(k)$. In order to ensure that Theorem 2 holds, the following inequality needs to be satisfied

$$\hat{\phi}_e^T(k+1)(I_N \otimes P_3)\hat{\phi}_e(k+1) \le I, \forall \hat{\phi}_e \in E_{tcs}. \tag{33}$$

Since E_{tcs} is a convex set, it can be replaced by $\forall \hat{\phi}_e \in \partial E_{tcs}(\hat{\phi}_e^T(k)(I_N \otimes P_3)\hat{\phi}_e(k) = I)$ instead of $\forall \hat{\phi}_e \in E_{tcs}$. Meanwhile, due to the convergence of $e_\phi(k)$ has been proved, it can be assumed that $\|e_\phi(k)\| \le \eta$. Based on Lemma 2.2 in [36], one gets

$$\begin{aligned}&\hat{\phi}_e^T(k)\Big(I_N \otimes (A_e - B_e K)^T P_3 (A_e - B_e K)\Big)\hat{\phi}_e(k) \\ &\quad + \frac{\eta}{\delta}\hat{\phi}_e^T(k)\left(M^T M \otimes \lambda_{\max 1} P_3\right)\hat{\phi}_e(k) \\ &\quad - \frac{1}{1+\delta}\hat{\phi}_e^T(k)(I_N \otimes P_3)\hat{\phi}_e(k) \le 0,\end{aligned} \tag{34}$$

where $\lambda_{\max 1} = \lambda_{\max}\left(C^T H^T P_3 HC\right)$ denotes the maximum eigenvalue of $C^T H^T P_3 HC$. Define $W_3 = P_3^{-1}$, the following

matrix inequality can be obtained according to Schur complement theorem and spectral decomposition

$$\begin{bmatrix} \frac{1}{\delta+1}\left(1-\frac{\eta(\delta+1)}{\delta}\lambda^2\lambda_{\max 1}\right)W_3 & * \\ (A_e-B_eK)W_3 & W_3 \end{bmatrix} \geq 0, \tag{35}$$

where $\lambda = \max\{\lambda_1, \lambda_2, \dots \lambda_N\}$, $\delta \in (0, \infty)$, $\lambda_{\max 1} \in \left(0, \frac{\delta}{\eta(\delta+1)\lambda^2}\right)$, and $\lambda_{\max 1} I - C^T H^T P_3 H C \geq 0$. Define $h = \frac{1}{\delta+1}\left(1-\frac{\eta(\delta+1)}{\delta}\lambda^2\lambda_{\max 1}\right)$, assuming that h is known, then one can obtain $\lambda_{\max 1} = \frac{\delta}{\eta\lambda^2(\delta+1)} - \frac{\delta}{\eta\lambda^2}h$. When $\delta = \frac{1}{\sqrt{h}} - 1$, $\lambda_{\max 1}$ takes its maximum value $\tilde{\lambda}_{\max 1} = \frac{1}{\eta\lambda^2}\left(1-\sqrt{h}\right)^2$. Thus, the matrix inequality constraint can be converted to

$$\begin{aligned} &\begin{bmatrix} hW_3 & * \\ (A_e-B_eK)W_3 & W_3 \end{bmatrix} \geq 0, \\ &\begin{bmatrix} \frac{1}{\eta\lambda^2}\left(1-\sqrt{h}\right)^2 I & * \\ HC & W_3 \end{bmatrix} \geq 0, \end{aligned} \tag{36}$$

where $h \in (0, 1)$. To obtain the maximum terminal constraint set, the optimization problem $\min \ -\log(\det W_3)$ can be solved while satisfying (36). ■

C. Proof of Theorem 3

Substituting the terminal controller (15) and overall closed-loop system (32) into (17). Since the convergence of $e_\phi(k)$ and $e_\delta(k)$ has been proved, and the disturbance $f_d(k)$ is L_2 bounded function, it follows that $f_d(k)$ is also a bounded function and satisfies $\left\|\hat{f}_d(k)\right\|_2 \leq \mu$. Performing the inequality transformation on (17), that is

$$\begin{aligned} &(1+\delta)\hat{\phi}_e^T(k)\left(I_N \otimes (A_e-B_eK)^T P_4 (A_e-B_eK)\right)\hat{\phi}_e(k) \\ &+\eta\left(1+\frac{1}{\delta}\right)\hat{\phi}_e^T(k)\left(M^TM \otimes \lambda_{\max 1}P_3\right)\hat{\phi}_e(k) \\ &-\hat{\phi}_e^T(k)\left(I_N \otimes P_4\right)\hat{\phi}_e(k) + \hat{\phi}_e^T(k)\left(I_N \otimes Q\right)\hat{\phi}_e(k) \\ &+\hat{\phi}_e^T(k)\left(M^TM \otimes H_2^TH_2\right)\hat{\phi}_e(k) \\ &+2\hat{\phi}_e^T(k)\left(I_N \otimes K^TRK\right)\hat{\phi}_e(k) \\ &+2\mu\hat{\phi}_e^T(k)\left(I_N \otimes \lambda_{\max}\left(H_1^TRH_1\right)P_3\right)\hat{\phi}_e(k) \leq 0. \end{aligned} \tag{37}$$

It should be noted that $\lambda_{\max}\left(H_1^TRH_1\right)$ does not involve the matrix variable and can be defined as $\sigma = \lambda_{\max}\left(H_1^TRH_1\right)$. The subsequent proof is similar to Theorem 2, defining $W_4 = P_4^{-1}$ and $\Upsilon = \left(P_3 + Q + \lambda^2 H_2^T H_2 + 2K^TRK + 2\mu\sigma P_3 - \sqrt{h}P_3\right)^{\frac{1}{2}}$, it can be concluded that

$$\begin{aligned} &\begin{bmatrix} \sqrt{h}W_4 & * & * \\ (A_e-B_eK)W_4 & W_4 & * \\ \Upsilon W_4 & 0 & \frac{1}{\sqrt{h}} \end{bmatrix} \geq 0, \\ &\begin{bmatrix} \frac{1}{\eta\lambda^2}\left(1-\sqrt{h}\right)^2 I & * \\ HC & W_4 \end{bmatrix} \geq 0. \end{aligned} \tag{38}$$

In order to minimize the terminal penalty matrix, the optimization problem $\min \ -\log(\det W_4)$ can be solved while satisfying (38). ■

Caoyuan Gu received the B.Eng. degree in electrical engineering and automation from China Jiliang University, HangZhou, China, in 2018.

He is currently pursuing a Ph.D. degree with the College of Information Engineering, Zhejiang University of Technology, Hangzhou, China. His research interests include cyber-physical systems, fault diagnosis and fault tolerant control.

Xiang Wu received the B.S. degree in automation, the M.S. degree in control engineering, and the Ph.D. degree in control theory and control engineering from the Zhejiang University of Technology, Hangzhou, China, in 2012, 2015, and 2020, respectively.

He is currently a Postdoctor with the College of Information Engineering, Zhejiang University of Technology. His research interests include disturbance rejection, networked motion-control systems, and cloud control systems.

Wen-An Zhang received the B.Eng. degree in automation and the Ph.D. degree in control theory and control engineering from the Zhejiang University of Technology, Hangzhou, China, in 2004 and 2010, respectively.

He is currently with the Department of Automation, Zhejiang University of Technology, Hangzhou, China. His research interests include networked control systems, multisensor information fusion estimation, and motion control.

Prof. Zhang has been a Subject Editor for Optimal Control Applications and Methods since September 2016.

Hongjie Ni received the B.S. degree in mechatronics from Hangzhou university of electronic science and technology, China, in 2003, and the M.S. degrees in Control Engineering from Zhejiang University of Technology, China, in 2008.

He is currently a Senior engineer in College of Information Engineering, Zhejiang University of Technology. His current research interests include Mechatronics, intelligent control of stage equipment.

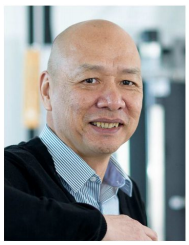

Steven X. Ding received the Ph.D. degree in electrical engineering from the Gerhard-Mercator University of Duisburg, Duisburg, Germany, in 1992.

From 1992 to 1994, he was an Research and Development Engineer with Rheinmetall GmbH, Germany. From 1995 to 2001, he was a Professor of control engineering with the University of Applied Science Lausitz, Senftenberg, Germany, where he served as the Vice President from 1998 to 2000.

He is currently a Full Professor of control engineering and the Head of the Institute for Automatic Control and Complex Systems (AKS), University of Duisburg-Essen, Duisburg.

His current research interests include model-based and data-driven fault diagnosis, fault-tolerant systems, real-time control, and their application in industry with a focus on automotive systems and chemical processes.